

Pr. Mauro Giudici
Editor HESS

Avignon, Ouargla, October 31th 2016

Dear Professor Giudici,

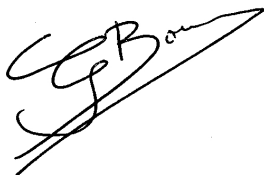
thank you very much for your comments and suggestions.

We modified our manuscript to show how it can be of interest to an international audience:

- the aquifers studied are important both quantitatively and as a scarce resource in a semi-arid to hyper-arid environment; there are very few studies on these aquifers;
- inverse modeling is used to quantitatively assess the modifications of the chemical composition of water along the flowpath combining mass transfer between aquifers and water and reactive mixing; isotope data are used to discriminate statistically equivalent models;
- the methodology and data can be integrated in a straightforward manner in a general framework where geochemical models (PhreeqC or others), crop models and land use models are operationally interfaced, as the achievement of cooperative efforts during the last decades referred to at the end of the introduction.

Modifications are not limited to the introduction and are shown by correction marks in the margins throughout the manuscript.

With our best regards,



Pr. Guilhem Bourri and Dr Rabia Slimani

1 Identification of dominant hydrogeochemical processes for
2 groundwaters in Algerian Sahara supported by inverse modeling
3 of chemical and isotopic data

4 R. Slimani^a, A. Guendouz^b, F. Trolard^c, A.S. Moulla^d, B. Hamdi-Aïssa^a, G. Bourrié^c

5 ^a*Ouargla University, Fac. des Sciences de la Nature et de la Vie, Lab. Biochimie des Milieux Désertiques, Ouargla*
6 *30000, Algeria*

7 ^b*Blida University, Science and Engineering Faculty, P.O.Box 270 Soumaa, Blida, Algeria*

8 ^c*INRA, UMR 1114 Emmah, Avignon, France*

9 ^d*Algiers Nuclear Research Centre, P.O. Box, 399 Alger-RP, 16000 Algiers, Algeria*

10 **Abstract**

Unpublished chemical and isotopic data taken in November 1992 from the three major Saharan aquifers namely, the “Continental Intercalaire” (CI), the “Complexe Terminal” (CT) and the Phreatic aquifer (Phr) were integrated with original samples in order to chemically and isotopically characterize the largest Saharan aquifer system and investigate the processes through which groundwaters acquire their mineralization. Instead of classical Debye-Hückel extended law, Specific Interaction Theory (SIT) model, recently incorporated in Phreeqc 3.0 was used. Inverse modeling of hydrochemical data constrained by isotopic data was used here to quantitatively assess the influence of geochemical processes: at depth, the dissolution of salts from the geological formations during upward leakage without evaporation explains the transitions from CI to CT and to a first end member, cluster of Phr (cluster I); near the surface, the dissolution of salts from sebkhas by rainwater explains another cluster of Phr (cluster II). In every case, secondary precipitation of calcite occurs during dissolution. All Phr waters result from the mixing of these two clusters together with calcite precipitation and ion exchange processes. These processes are quantitatively assessed by Phreeqc model. Globally, gypsum dissolution and calcite precipitation were found to act as a carbon sink.

11 *Keywords:* hydrochemistry, stable isotopes, Sahara, Algeria

12 **1. INTRODUCTION**

13 A scientific study published in 2008 (OECD, 2008) showed that 85% of the world population
14 lives in the driest half of the earth. More than 1 billion people residing in arid and semi-arid areas
15 of the world have access to only few or non-renewable water resources. [The North-Western](#)
16 [Sahara Aquifer System \(NWSAS\)](#) is one of the largest captive reservoirs in the world and its
17 [huge water reserves](#) are essentially composed of an old component. It is represented by two
18 [main deep aquifers](#), the [Continental Intercalaire](#) and the [Complexe Terminal](#). This system covers

Email address: slm_rabia@yahoo.fr (R. Slimani)

19 a surface area of more than one million km² of which 700,000 km² are in Algeria, 80,000 km²
20 in Tunisia and 250,000 km² in Libya. With regard to the climatic conditions of the Sahara,
21 these formations are poorly renewed: about 1 billion m³/year total essentially infiltrated in the
22 Piedmont of the Saharan Atlas in Algeria, as well as in the Dahar and Djebel Nafusa in Tunisia
23 and Libya respectively. However, the very large expansion of the system as well as the great
24 thickness of the aquifer layers has favored the accumulation of huge water reserves. Ouargla
25 basin occurs right in the middle of the NWSAS and thus benefits from its Groundwater resources
26 (Fig. 1) are contained in three main reservoirs (UNESCO, 1972; Eckstein and Eckstein, 2003;
27 OSS, 2003, 2008). These are namely:

- 28 • at the top, the phreatic aquifer (Phr), in the Quaternary sandy gypsum permeable forma-
29 tions of Quaternary, is almost unexploited, due to its extreme salinity (50 g/L);
- 30 • in the middle, the “Complexe Terminal” (CT) (Cornet and Gouscov, 1952; UNESCO,
31 1972) is the most exploited and includes several aquifers in different geological formations.
32 Groundwater circulates in one or the two lithostratigraphic formations of the Eocene and
33 Senonian carbonates or in the Mio-pliocene sands;
- 34 • at the bottom, the “Continental Intercalaire” (CI), hosted in the lower Cretaceous continen-
35 tal formations (Barremian and Albian), mainly composed of sandstones, sands and clays.
36 It is only partially exploited because of its significant depth.

37 The integrated management of these groundwaters is presently a serious issue for local water
38 resources managers due to the large extension of the aquifers and the complexity of the relations
39 between them. Several studies (Guendouz, 1985; Fontes et al., 1986; Guendouz and Moulla,
40 1996; Edmunds et al., 2003; Guendouz et al., 2003; Hamdi-Aïssa et al., 2004; Foster et al.,
41 2006; OSS, 2008) started from chemical and isotopic information (²H, ¹⁸O, ²³⁴U, ²³⁸U, ³⁶Cl)
42 to characterize the relationships between aquifers. In particular, such studies focused on the
43 recharge of the deep CI aquifer system. These investigations especially dealt with water chemi-
44 cal facies, mapped isocontents of various parameters, and reported typical geochemical ratios
45 ($[\text{SO}_4^{2-}]/[\text{Cl}^-]$, $[\text{Mg}^{2+}]/[\text{Ca}^{2+}]$) as well as other correlations. Minerals / solutions equilibria were
46 checked by computing saturation indices with respect to calcite, gypsum, anhydrite and halite,
47 but processes were only *qualitatively* assessed.

48 The present study aims at applying for the first time ever in Algeria, inverse modeling to an
49 extreme environment, featured by a lack of data on a scarce natural resource (groundwater). New
50 data were hence collected in order to characterize the hydrochemical and the isotopic composi-
51 tion of the major aquifers in the Saharan region of Ouargla. New possibilities offered by progress
52 in geochemical modeling were used. The objective was also to identify the origin of the mineral-
53 ization and the water-rock interactions that occur along the flowpath. More specifically, inverse
54 modeling of chemical reactions allows one to select the best conceptual model for the interpre-
55 tation of the geochemical evolution of Ouargla aquifer system. The stepwise inversion strategy
56 involves designing a list of scenarios (hypotheses) that take into consideration the most plausible
57 combinations of geochemical processes that may occur within the studied medium. After resolv-
58 ing the scenarios in a stepwise manner, the one that provides the best conceptual geochemical
59 model is then selected, which allowed (Dai et al., 2006) to optimize simultaneously transmissiv-
60 ities and geochemical transformations in a confined aquifer. Inverse modeling with Phreeqc 3.0
61 was used here in a different way, only on geochemical data but for several aquifers, to account for
62 the modifications of the composition of water along the flowpath. At least two chemical analyses

63 of groundwater at different points of the flow path, and a set of phases (minerals and/ or gases)
64 which potentially react while water circulates are needed to operate the program (Charlton et al.,
65 1996).

66 A number of assumptions are inherent to the application of inverse geochemical modeling:
67 (i) the two groundwater analyses from the initial and the final boreholes should represent ground-
68 water that flows along the same flow path, (ii) dispersion and diffusion do not significantly affect
69 groundwater chemistry, (iii) a chemical steady-state prevails in the groundwater system during the
70 time considered, and (iv) the mineral phases used in the inverse calculation are or were present in
71 the aquifer (Zhu and Anderson, 2002). The soundness or the validity of the results depends on a
72 valid conceptualization of the groundwater system, on the validity of the basic hydrogeochemical
73 concepts and principles, and on the accuracy of model input data, and the level of understanding
74 of the geochemical processes occurring in the area (Güler and Thyne, 2004; Sharif et al., 2008).
75 These requirements are fulfilled in the region of Ouargla, which can be considered as a “win-
76 dow” open on the largest Saharan aquifer, and thus one of the largest aquifers in the world in a
77 semi-arid to hyper-arid region subject to both global changes: urban sprawl and climate change.
78 The methodology developed here and the data collected can easily be integrated in the PRECOS
79 framework proposed for the management of environmental resources (Trolard et al., 2016).

80 2. METHODOLOGY

81 2.1. Presentation of the study area

82 The study area is located in the northeastern desert of Algeria “Lower-Sahara” (Le Houérou,
83 2009) near the city of Ouargla (Fig. 1), 31°54' to 32°1' N and 5°15' to 5°27' E, with a mean ele-
84 vation of 134 (m.a.s.l.). It is located in the quaternary valley of Oued Mya basin. Present climate
85 belongs to the arid Mediterranean-type (Dubief, 1963; Le Houérou, 2009; ONM, 1975/2013), as
86 it is characterized by a mean annual temperature of 22.5 °C, a yearly rainfall of 43.6 mm/yr and
87 a very high evaporation rate of 2,138 mm/yr.

88 Ouargla's region and the entire Lower Sahara has experienced during its long geological history
89 alternating marine and continental sedimentation phases. During Secondary era, vertical move-
90 ments affected the Precambrian basement causing in particular collapse of its central part, along
91 an axis passing approximately through the Oued Righ valley and the upper portion of the val-
92 ley oued Mya. According to Furon (1960), an epicontinental sea spread to the Lower Eocene of
93 northern Sahara. After the Oligocene, the sea gradually withdrew. It is estimated at present that
94 this sea did not reach Ouargla and transgression stopped at the edge of the bowl (Furon, 1960;
95 Lelièvre, 1969). The basin is carved into Mio-pliocene (MP) deposits, which alternate with red
96 sands, clays and sometimes marls; gypsum is not abundant and dated from Pontian (MP) (Cornet
97 and Gouscov, 1952; Dubief, 1953; Ould Baba Sy and Besbes, 2006). The continental Pliocene
98 consists of a local limestone crust with puddingstone or lacustrine limestone (Fig. 2), shaped
99 by eolian erosion into flat areas (regs). The Quaternary formations are lithologically composed
100 of alternating layers of permeable sand and relatively impermeable marl (Aumassip et al., 1972;
101 Chellat et al., 2014).

102 The exploitation of Mio-pliocene aquifer is ancient and at the origin of the creation of the
103 oasis (Lelièvre, 1969; Moulias, 1927). The piezometric level was higher (145 m a.s.l.) but over-
104 exploitation at the end of the XIXth century led to a catastrophic decrease of the resource, with
105 presently more than 900 boreholes (ANRH, 2011).

106 The exploitation of Senonian aquifer dates back to 1953 at a depth between 140 to 200 m,
107 with a small initial rate *ca.* 9 L s^{-1} ; two boreholes have been exploited since 1965 and 1969, with
108 a total flowrate *ca.* 42 L s^{-1} , for drinking water and irrigation.

109 The exploitation of Albian aquifer dates back to 1956, presently, two boreholes are exploited:

- 110 • El Hedeb I, 1,335 m deep, with a flowrate 141 L s^{-1} ;
- 111 • El Hedeb II, 1,400 m deep, with a flowrate 68 L s^{-1} .

112 2.2. Sampling and analytical methods

113 The sampling programme consisted of collecting samples along transects corresponding to
114 directions of flow for both Phr and CT aquifers while it was possible to collect only eight samples
115 from the CI. A total of 107 samples were collected during a field campaign in 2013, along the
116 main flowpath of Oued Mya. 67 of them were from piezometers tapping the phreatic aquifer,
117 32 from CT wells and the last 8 from boreholes tapping the CI aquifer (Fig. 3). Analyses of
118 Na^+ , K^+ , Ca^{2+} , Mg^{2+} , Cl^- , SO_4^{2-} and HCO_3^- were performed by ion chromatography at Algiers
119 Nuclear Research Center (CRNA). Previous and yet unpublished data (Guendouz and Moulla,
120 1996) sampled in 1992 are used here too: 59 samples for Phr aquifer, 15 samples for CT aquifer
121 and 3 samples for the CI aquifer for chemical analyses, data ^{18}O and ^3H (Guendouz and Moulla,
122 1996).

123 2.3. Geochemical method

124 Phreeqc was used to check minerals / solution equilibria using the specific interaction the-
125 ory (SIT), *i.e.* the extension of Debye-Hückel law by Scatchard and Guggenheim incorporated
126 recently in Phreeqc 3.0 (Parkhurst and Appelo, 2013). Inverse modeling was used to calculate
127 the number of minerals and gases' moles that must respectively dissolve or precipitate/degas to
128 account for the difference in composition between initial and final water end members (Plum-
129 mer and Back, 1980; Kenoyer and Bowser, 1992; Deutsch, 1997; Plummer and Sprinkle, 2001;
130 Güler and Thyne, 2004; Parkhurst and Appelo, 2013). This mass balance technique has been
131 used to quantify reactions controlling water chemistry along flow paths (Thomas et al., 1989).
132 It is also used to quantify the mixing proportions of end-member components in a flow system
133 (Kuells et al., 2000; Belkhiri et al., 2010, 2012).

134 Inverse modeling involves designing a list of scenarios (modelling setups) that take into ac-
135 count the most plausible combinations of geochemical processes that are likely to occur in our
136 system. For example, the way to identify whether calcite dissolution/precipitation is relevant or
137 not consists of solving the inverse problem under two alternate scenarios: (1) considering a geo-
138 chemical system in which calcite is present, and (2) considering a geochemical system without
139 calcite. After simulating the two scenarios, it is usually possible to select the setup that gives the
140 best results as the solution to the inverse modeling according to the fit between the modeled and
141 observed values. Then one can conclude whether calcite dissolution/precipitation is relevant or
142 not. This stepwise strategy allows us to identify the relevance of a given chemical process by
143 inversely solving the problem through alternate scenarios in which the process is either partici-
144 pating or not (Dai et al., 2006).

145 In geochemical modeling inverse, soundness of results are dependent upon valid conceptu-
146 alization of the system, validity of basic concepts and principles, accuracy of input data, and
147 level of understanding of the geochemical processes. We use the information from the lithology,
148 general hydrochemical evolution patterns, saturation indices and mineral stability diagrams to
149 constrain the inverse models.

150 3. RESULTS AND DISCUSSION

151 Tables 1 to 4 illustrate the results of the chemical and the isotopic analyses. Samples are
152 ordered according to an increasing electric conductivity (EC), and this is assumed to provide
153 an ordering for increasing salt content. In both phreatic and CT aquifers, temperature is close to
154 25 °C, while for CI aquifer, temperature is close to 50 °C. The values presented in tables 1 to 5 are
155 raw analytical data that were corrected for defects of charge balance before computing activities
156 with Phreeqc. As analytical errors could not be ascribed to a specific analyte, the correction was
157 made proportionally. The corrections do not affect the anions to anions mole ratios such as for
158 $[\text{HCO}_3^-]/([\text{Cl}^-] + 2[\text{SO}_4^{2-}])$ or $[\text{SO}_4^{2-}]/[\text{Cl}^-]$, whereas they affect the cation to anion ratio such
159 as for $[\text{Na}^+]/[\text{Cl}^-]$.

160 3.1. Characterization of chemical facies of the groundwater

161 Piper diagrams drawn for the studied groundwaters (Fig. 4) broadly show a scatter plot dom-
162 inated by a Chloride-Sodium facies. However, when going into small details, the widespread
163 chemical facies of the Phr aquifer is closer to the NaCl cluster than those of CI and CT aquifers.
164 Respectively, CaSO_4 , Na_2SO_4 , MgSO_4 and NaCl are the most dominant chemical species (min-
165 erals) that are present in the phreatic waters. This sequential order of solutes is comparable to
166 that of other groundwater occurring in North Africa, and especially in the neighboring area of
167 the chotts (depressions where salts concentrate by evaporation) Merouane and Melrhir (Vallès
168 et al., 1997; Hamdi-Aïssa et al., 2004).

169 3.2. Spatial distribution of the mineralization

170 The salinity of the phreatic aquifer varies considerably depending on the location (namely,
171 the distance from wells or drains) and time (due to the influence of irrigation) (Fig. 5a).

172 Its salinity is low around irrigated and fairly well-drained areas, such as the palm groves of
173 Hassi Miloud, just north of Ouargla (Fig. 3) that benefit from freshwater and are drained to the
174 sebkha Oum el Raneb. However, the three lowest salinity values are observed in the wells of
175 Ouargla palm-grove itself, where the Phr aquifer watertable is deeper than 2 m.

176 Conversely, the highest salinity waters are found in wells drilled in the chotts and sebkhas (a
177 sebkha is the central part of a chott where salinity is the largest) (Safioune and Oum er Raneb)
178 where the aquifer is often shallower than 50 cm.

179 The salinity of the CT (Mio-pliocene) aquifer (Fig. 5b) is much lower than that of the Phr
180 aquifer, and ranges from 1 to 2 g/L; however, its hardness is larger and it contains more sulfate,
181 chloride and sodium than the waters of the Senonian formations and those of the CI aquifer. The
182 salinity of the Senonian aquifer ranges from 1.1 to 1.7 g/L, while the average salinity of the CI
183 aquifer is 0.7 g/L (Fig. 5c).

184 A likely contamination of the Mio-pliocene aquifer by phreatic groundwaters through casing
185 leakage in an area where water is heavily loaded with salt and therefore particularly aggressive
186 cannot be excluded.

187 3.3. Saturation Indices

188 The calculated saturation indices (SI) reveal that waters from CI at 50 °C are close to equi-
189 librium with respect to calcite, except for 3 samples that are slightly oversaturated. They are
190 however all undersaturated with respect to gypsum (Fig. 6).

191 Moreover, they are oversaturated with respect to dolomite and undersaturated with respect to
192 anhydrite and halite (Fig. 7).

193 Waters from CT and phreatic aquifers show the same pattern, but some of them are more
194 largely oversaturated with respect to calcite, at 25 °C.

195 However, several phreatic waters (P031, P566, PLX4, PL18, P002, P023, P116, P066, P162
196 and P036) that are located in the sebkhas of Sefioune, Oum-er-Raneb, Bamendil and Ain el
197 Beida's chott are saturated with gypsum and anhydrite. This is in accordance with highly evapo-
198 rative environments found elsewhere (UNESCO, 1972; Hamdi-Aïssa et al., 2004; Slimani, 2006).

199 No significant trend of SI from south to north upstream and downstream of Oued Mya (Fig. 7)
200 is observed. This suggests that the acquisition of mineralization is due to geochemical processes
201 that have already reached equilibrium or steady state in the upstream areas of Ouargla.

202 3.4. *Change of facies from the carbonated cluster to the evaporites' cluster*

203 The facies shifts progressively from the carbonated (CI and CT aquifers) to the evaporites'
204 one (Phr aquifer) with an increase in sulfates and chlorides at the expense of carbonates (SI
205 of gypsum, anhydrite and halite). This is illustrated by a decrease of the $[\text{HCO}_3^-]/([\text{Cl}^-] +$
206 $2[\text{SO}_4^{2-}])$ ratio (Fig. 8) from 0.2 to 0 and of the $[\text{SO}_4^{2-}]/[\text{Cl}^-]$ ratio from 0.8 to values smaller
207 than 0.3 (Fig. 9) while salinity increases. Carbonate concentrations tend towards very small
208 values, while it is not the case for sulfates. This is due to both gypsum dissolution and calcite
209 precipitation. Chlorides in groundwater may come from three different sources: (i) ancient sea
210 water entrapped in sediments; (ii) dissolution of halite and related minerals that are present in
211 evaporite deposits and (iii) dissolution of dry fallout from the atmosphere, particularly in these
212 arid regions (Matiatos et al., 2014; Hadj-Ammar et al., 2014).

213 $[\text{Na}^+]/[\text{Cl}^-]$ ratio ranges from 0.85 to 1.26 for CI aquifer, from 0.40 to 1.02 for the CT aquifer,
214 from 0.13 to 2.15 for the Phr aquifer. The measured points from the three considered aquifers
215 are linearly scattered with good approximation around the unity slope straight line that stands
216 for halite dissolution (Fig. 10). The latter appears as the most dominant reaction occurring in
217 the medium. However, at very high salinity, Na^+ seems to swerve from the straight line, towards
218 smaller values.

219 A further scrutiny of Fig. 10 shows that CI waters are very close to the 1:1 line. CT waters
220 are enriched in both Na^+ and Cl^- but slightly lower than the 1:1 line while phreatic waters are
221 largely enriched and much more scattered. CT waters are closer to the seawater mole ratio
222 (0.858), but some lower values imply a contribution from another source of chloride than halite
223 or from entrapped seawater. Conversely, a $[\text{Na}^+]/[\text{Cl}^-]$ ratio larger than 1 is observed for phreatic
224 waters, which implies the contribution of another source of sodium, most likely sodium sulfate,
225 that is present as mirabilite or thenardite in the chotts and the sebkhas areas.

226 $[\text{Br}^-]/[\text{Cl}^-]$ ratio ranges from 2×10^{-3} to 3×10^{-3} . The value of this molar ratio for halite is
227 around 2.5×10^{-3} , which matches the aforementioned range and confirms that halite dissolution
228 is the most dominant reaction taking place in the studied medium.

229 In the CI, CT and Phr aquifers, calcium originates both from carbonate and sulfate (Fig. 11
230 and 12). Three samples from CI aquifer are close to the $[\text{Ca}^{2+}]/[\text{HCO}_3^-]$ 1:2 line, while calcium
231 sulfate dissolution explains the excess of calcium. However, nine samples from Phr aquifer are
232 depleted in calcium, and plot under the $[\text{Ca}^{2+}]/[\text{HCO}_3^-]$ 1:2 line. This cannot be explained by
233 precipitation of calcite, as some are undersaturated with respect to that mineral, while others are
234 oversaturated.

235 In this case, a cation exchange process seems to occur and lead to a preferential adsorption
236 of divalent cations, with a release of Na^+ . This is confirmed by the inverse modeling that is
237 developed below and which implies Mg^{2+} fixation and Na^+ and K^+ releases.

238 Larger sulfate values observed in the phreatic aquifer (Fig. 12) with $[\text{Ca}^{2+}]/[\text{SO}_4^{2-}] < 1$ can
 239 be attributed to a Na-Mg sulfate dissolution from a mineral bearing such elements. This is for
 240 instance the case of bloedite.
 241

242 3.5. Isotope geochemistry

243 CT and CI aquifer exhibit depleted and homogeneous ^{18}O contents, ranging from -8.32‰
 244 to -7.85‰ . This was already previously reported by many authors (Edmunds et al., 2003;
 245 Guendouz et al., 2003; Moulla et al., 2012). On the other hand, ^{18}O values for the phreatic
 246 aquifer are widely dispersed and vary between -8.84‰ to 3.42‰ (Table 5). Waters located
 247 north of the virtual line connecting approximately Hassi-Miloud to sebkhet Safioune, are found
 248 more enriched in heavy isotopes and are thus more evaporated. In that area, water table is close to
 249 the surface and mixing of both CI and CT groundwaters with phreatic ones through irrigation is
 250 nonexistent. Conversely, waters located south of Hassi Miloud up to Ouargla city show depleted
 251 values. This is the clear fingerprint of a contribution to the Phr waters from the underlying CI
 252 and CT aquifers (Gonfiantini et al., 1975; Guendouz, 1985; Fontes et al., 1986; Guendouz and
 253 Moulla, 1996).

254 Phreatic waters result from a mixing of two end-members. An evidence for this is given by
 255 considering the $([\text{Cl}^-], ^{18}\text{O})$ relationship (Fig. 13). The two clusters are: i) a first cluster of ^{18}O
 256 depleted groundwater (Fig. 14), and ii) another cluster of ^{18}O enriched groundwater with positive
 257 values and a high salinity. The latter is composed of phreatic waters occurring in the northern
 258 part of the study region.

259 Cluster I represents the waters from CI and CT whose isotopic composition is depleted
 260 in ^{18}O (average value around -8.2‰) (Fig. 13). They correspond to an old water recharge
 261 (palæorecharge); whose age estimated by means of ^{14}C , exceeds 15.000 years BP (Guendouz,
 262 1985; Guendouz and Michelot, 2006). So, it is not a water body that is recharged by recent
 263 precipitation. It consists of CI and CT groundwaters and partly of phreatic waters, and can be
 264 ascribed to an upward leakage favored by the extension of faults near Amguid El-Biod dorsal.

265 Cluster II, observed in Sebkhet Safioune, can be ascribed to the direct dissolution of surficial
 266 evaporitic deposits conveyed by evaporated rainwater.

267 Evaporation alone cannot explain the distribution of data that is observed (Fig. 13). An
 268 evidence for this is given in a semi-logarithmic plot (Fig. 14), as classically obtained according
 269 to the simple approximation of Rayleigh equation (cf. Appendix):

$$\delta^{18}\text{O} \approx 1000 \times (1 - \alpha) \log[\text{Cl}^-] + k, \quad (1)$$

$$\approx -\epsilon \log[\text{Cl}^-] + k, \quad (2)$$

270 where α is the fractionation factor during evaporation, $\epsilon \equiv -1000 \times (1 - \alpha)$ is the enrichment
 271 factor and k is a constant (Ma et al., 2010; Chkir et al., 2009). CI and CT waters are better
 272 separated in the semi-logarithmic plot because they are differentiated by their chloride content.
 273 According to equation (1), simple evaporation gives a straight line (solid line in Fig. 14). The
 274 value of ϵ used is the value at 25°C , which is equal to -73.5 .

275 P115 is the only sample that appears on the straight evaporation line (Fig. 14). It should be
 276 considered as an outlier since the rest of the samples are all well aligned on the logarithmic fit
 277 derived from the mixing line of Figure 13.

278 The phreatic waters that are close to cluster I (Fig. 13) correspond to groundwaters occurring in the edges of the basin (Hassi Miloud, piezometer P433) (Fig. 14). They are low-mineralized and acquire their salinity via two processes, namely: dissolution of evaporites along their underground transit up to Sebkhet Safioune and dilution through upward leakage by the less-mineralized waters of CI and CT aquifers (for example Hedeb I for CI and D7F4 for CT) (Fig. 14) (Guendouz, 1985; Guendouz and Moulla, 1996).

284 The rates of the mixing that are due to upward leakage from CI to CT towards the phreatic aquifer can be calculated by means of a mass balance equation. It only requires knowing the δ values of each fraction that is involved in the mixing process.

287 The δ value of the mixture is given by:

$$\delta_{\text{mix}} = f \times \delta_1 + (1 - f) \times \delta_2 \quad (3)$$

288 where f is the fraction of CI aquifer, $1 - f$ the fraction of the CT and δ_1 , δ_2 are the respective isotope contents.

290 Average values of mixing fractions from each aquifer to the phreatic waters computed by means of equation (3) gave the rates of 65 % for CI aquifer and 35% for CT aquifer.

292 A mixture of a phreatic water component that is close to cluster I (*i.e.* P433) with another component which is rather close to cluster II (*i.e.* P039) (Fig. 13 and 14), for an intermediate water with a $\delta^{18}\text{O}$ signature ranging from -5‰ to -2‰ gives mixture fraction values of 52 % for cluster I and 48 % for cluster II. Isotope results will be used to independently cross-check the validity of the mixing fractions derived from an inverse modeling involving chemical data (see section 3.6).

298 Turonian evaporites are found to lie in between CI deep aquifer and the Senonian and Miocene formations bearing CT aquifer. CT waters can thus simply originate from ascending CI waters that dissolve Turonian evaporites, a process which does not involve any change in ^{18}O content. Conversely, phreatic waters result to a minor degree from evaporation and mostly from dissolution of sebkhas evaporites by ^{18}O enriched rainwater and mixing with CI-CT waters.

303 3.5.1. Tritium content of water

304 Tritium contents of Phr aquifer are relatively small (Table 5), they vary between 0 and 8 TU. Piezometers PZ12, P036 and P068 show values close to 8 TU, piezometers P018, P019, P416, P034, P042 and P093 exhibit values ranging between 5 and 6 TU, and the rest of the samples' concentrations are lower than 2 TU.

308 These values are dated back to November 1992 so they are old values and they are considered high comparatively to what is expected to be found nowadays. In fact, at present times, tritium figures have fallen lower than 5 TU in precipitation measured in the northern part of the country.

311 Tritium content of precipitation was measured as 16 TU in 1992 on a single sample that was collected from the National Agency for Water Resources station in Ouargla. A major part of this rainfall evaporates back into the atmosphere that is unsaturated in moisture. Consequently, enrichment in tritium happens as water evaporates back. The lightest fractions (isotopes) are the ones that escape first causing enriching the remaining fraction in tritium. The 16 TU value would thus correspond to a rainy event that had happened during the field campaign (5, 6 Nov. 1992). It is the most representative value for that region and for that time. Unfortunately, all the other stations (Algiers, Ankara, and Tenerife) (Martinelli et al., 2014) are subject to a completely different climatic regime and besides the fact that they have more recent values, can absolutely not be used for our case. Therefore all the assumptions based on recent tritium rain values do not apply to this study.

322 Depleted contents in ^{18}O and low tritium concentrations for phreatic waters fit well the mix-
323 ing scheme and confirm the contribution from the older and deeper CI/CT groundwaters. The
324 affected areas were clearly identified in the field and correspond to locations that are subject to
325 a recycling and a return of irrigation waters whose origin are CI/CT boreholes. Moreover, the
326 mixing that is clearly brought to light by the Cl^- vs. ^{18}O diagrams (Fig. 13 and 14) could partly
327 derive from an ascending drainage from the deep and confined CI aquifer (exhibiting depleted ho-
328 mogenous ^{18}O contents and very low tritium), a vertical leakage that is favoured by the Amguid
329 El-biod highly faulted area (Guendouz and Moulla, 1996; Edmunds et al., 2003; Guendouz et al.,
330 2003; Moulla et al., 2012).

331 3.6. Inverse modeling

332 We assume that the relationship between ^{18}O and Cl^- data obtained in 1992 is stable with
333 time, which is a logical assumption as times of transfer from CI to both CT and Phr are very long.
334 Considering both ^{18}O and Cl^- data, CI, CT and Phr data populations can be categorized. The CI
335 and CT do not show appreciable ^{18}O variations, and can be considered as a single population. The
336 Phr samples consist however of different populations: cluster I, with $\delta^{18}\text{O}$ values close to -8, and
337 small Cl^- concentrations, more specifically less than 35 mmol L^{-1} ; cluster II, with $\delta^{18}\text{O}$ values
338 larger than 3, and very large Cl^- concentrations, more specifically larger than $4,000 \text{ mmol L}^{-1}$
339 (Table 6); intermediate Phr samples result from mixing between clusters I and II (mixing line in
340 Fig. 13, mixing curve in Fig. 14) and from evaporation of cluster I (evaporation line in Fig. 14).
341 The mass-balance modeling has shown that relatively few phases are required to derive observed
342 changes in water chemistry and to account for the hydrochemical evolution in Ouargla's region.
343 The mineral phases' selection is based upon geological descriptions and analysis of rocks and
344 sediments from the area (OSS, 2003; Hamdi-Aïssa et al., 2004).

345 The inverse model was constrained so that mineral phases from evaporites including gypsum,
346 halite, mirabilite, glauberite, sylvite and bloedite were set to dissolve until they reach saturation,
347 and calcite, dolomite were set to precipitate once they reached saturation. Cation exchange reac-
348 tions of Ca^{2+} , Mg^{2+} , K^+ and Na^+ on exchange sites were included in the model to check which
349 cations are adsorbed or desorbed during the process. Dissolution and desorption contribute as
350 positive terms in the mass balance, as elements are released in solution. On the other hand,
351 precipitation and adsorption contribute as negative terms, while elements removed from the so-
352 lution. $\text{CO}_{2(\text{g})}$ dissolution is considered by Phreeqc as a dissolution of a mineral, whereas $\text{CO}_{2(\text{g})}$
353 degassing is dealt with as if it were a mineral precipitation.

354 Inverse modelling leads to a quantitative assessment of the different solutes' acquisition pro-
355 cesses and a mass balance for the salts that are dissolved or precipitated from CI, CT and Phr
356 groundwaters (Fig. 14, Table 7), as follows:

- 357 • transition from CI to CT involves gypsum, halite and sylvite dissolution, and some ion
358 exchange namely calcium and potassium fixation on exchange sites against magnesium
359 release, with a very small and quite negligible amount of $\text{CO}_{2(\text{g})}$ degassing. The maximum
360 elemental concentration fractional error equals 1%. The model consists of a minimum
361 number of phases (*i.e.* 6 solid phases and $\text{CO}_{2(\text{g})}$); Another model implies as well dolomite
362 precipitation with the same fractional error;
- 363 • transition from CT to an average water component of cluster I involves dissolution of
364 halite, sylvite, and bloedite from Turonian evaporites, with a very tiny calcite precipitation.
365 The maximum fractional error in elemental concentration is 4%. Another model implies

366 $\text{CO}_{2(g)}$ escape from the solution, with the same fractional error. Large amounts of Mg^{2+}
367 and SO_4^{2-} are released within the solution (Sharif et al., 2008; Li et al., 2010; Carucci
368 et al., 2012);

369 • the formation of Phr cluster II can be modeled as being a direct dissolution of salts from the
370 sebkha by rainwater with positive $\delta^{18}\text{O}$; the most concentrated water (P036 from Sebkhet
371 Safioune) is taken here for cluster II, and pure water as rainwater. In a descending order
372 of amount, halite, sylvite, gypsum and huntite are the minerals that are the most involved
373 in the dissolution process. A small amount of calcite precipitates while some Mg^{2+} are
374 released versus K^+ fixation on exchange sites. The maximum elemental fractional error in
375 the concentration is equal to 0.004%. Another model implies dolomite precipitation with
376 some more huntite dissolving, instead of calcite precipitation, but salt dissolution and ion
377 exchange are the same. Huntite, dolomite and calcite stoichiometries are linearly related,
378 so both models can fit field data, but calcite precipitation is preferred compared to dolomite
379 precipitation at low temperature;

380 • the origin of all phreatic waters can be explained by a mixing in variable proportions
381 of cluster I and cluster II. For instance, waters from cluster I and cluster II can easily be
382 separated by their $\delta^{18}\text{O}$ respectively close to -8‰ and 3.5‰ (Fig. 13 and 14). Mixing the
383 two clusters is of course not an inert reaction, but rather results in the dissolution and the
384 precipitation of minerals. Inverse modeling is then used to compute both mixing rates and
385 the extent of matter exchange between soil and solution. For example, a phreatic water
386 (piezometer P068) with intermediate values ($\delta^{18}\text{O} = -3$ and $[\text{Cl}^-] \simeq 2\text{ M}$) is explained
387 by the mixing of 58% water from cluster I and 42% from cluster II. In addition, calcite
388 precipitates, Mg^{2+} fixes on exchange sites, against Na^+ and K^+ , gypsum dissolves as well
389 as a minor amount of huntite (Table 7). The maximum elemental concentration fractional
390 error is 2.5% and the mixing fractions' weighted $\delta^{18}\text{O}$ is -3.17‰ , which is very close to
391 the measured value (-3.04‰). All the other models, making use of a minimum number of
392 phases, and not taking into consideration ion exchange reactions are not found compatible
393 with isotope data. Mixing rates obtained with such models are for example 98% of cluster
394 I and 0.9% of cluster II, which leads to a $\delta^{18}\text{O} = (-7.80\text{‰})$ which is quite far for the real
395 measured value (-3.04‰).

396 The main types of groundwaters occurring in Ouargla basin are thus explained and could
397 quantitatively be reconstructed. An exception is however sample P115, which is located exactly
398 on the evaporation line of Phr cluster I. Despite numerous attempts, it could not be quantitatively
399 rebuilt. Its ^3H value (6.8) indicates that it is derived from a more or less recent water component
400 with very small salt content, most possibly affected by rainwater and some preferential flow
401 within the piezometer. As this is the only sample on this evaporation line, there remains a doubt
402 on its significance.

403 Globally, the summary of mass transfer reactions occurring in the studied system (Table 7)
404 shows that gypsum dissolution results in calcite precipitation and $\text{CO}_{2(g)}$ dissolution, thus acting
405 as an inorganic carbon sink.

406 4. CONCLUSIONS

407 From the three aquifers studied here, two (Complexe Terminal) and (Continental Intercalaire)
408 are the main aquifers of Sahara, by the extent (thousands of km from the recharge area to the Gulf

409 of Gabès) and time of transfer (thousands of years). The last one, Phreatic aquifer, is shallow.
410 The chemical facies have long been qualitatively described. Our results explain for the first time
411 quantitatively the processes that occur during upward leakage through interaction between solu-
412 tion and the mineral constituents of the aquifers, and ultimately by mixing with surface waters.
413 The hydrochemical study of the aquifer system occurring in Ouargla's basin allowed us to iden-
414 tify the origin of its mineralization. Waters exhibit two different facies: sodium chloride and
415 sodium sulfate for the phreatic aquifer (Phr), sodium sulfate for the Complexe Terminal (CT)
416 aquifer and sodium chloride for the Continental Intercalaire (CI) aquifer. Calcium carbonate
417 precipitation and evaporite dissolution explain the facies change from carbonate to sodium chlo-
418 ride or sodium sulfate that is recorded. However, reactions imply many minerals with common
419 ions, deep reactions without evaporation as well as shallow processes affected by both evapora-
420 tion and mixing. Those processes are separated by considering both chemical and isotopic data,
421 and quantitatively explained making use of an inverse geochemical modeling. The latter was ap-
422 plied for the first time ever in Algeria, to an extreme environment, featured by a lack of data on
423 a scarce natural resource such as Saharan groundwater. This methodology brought added-value
424 to the comprehension of the processes occurring within the studied groundwaters on which the
425 populations of the region rely for their daily consumption as well as for their agriculture directed
426 mainly towards the culture of the main product of such an area that is dates besides at a lower
427 extent other sub-products such as vegetables within the date-palms groves themselves. Results
428 obtained through inverse modeling could help water resources' managers both at the local and
429 the regional scales, to gather the necessary information for an integrated management of that
430 vital resource. Moreover and regarding the large geographic scale of the aquifers, such a pilot
431 study could be taken as a support work to further investigations elsewhere in similar regions. The
432 present study leads to the main result that phreatic waters do not originate simply from infiltra-
433 tion of rainwater and dissolution of salts from the sebkhas. Conversely, Phr waters are largely
434 influenced by the upwardly mobile deep CT and CI groundwaters, fractions of the latter interact-
435 ing with evaporites from the Turonian formations. Phreatic waters occurrence is explained as a
436 mixture of two end-member components: cluster I, which is very close to CI and CT, and cluster
437 II, which is highly mineralized and results from the dissolution by rainwater of salts from the
438 sebkhas. At depth, CI leaks upwardly and dissolves gypsum, halite and sylvite, with some ion
439 exchange, to give waters of CT aquifer composition. CT transformation into Phr cluster I waters
440 involves the dissolution of Turonian evaporites (halite, sylvite and bloedite) with minor calcite
441 precipitation.

442 At the surface, direct dissolution by rainwater of salts from sebkhas (halite, sylvite, gypsum
443 and some huntite) with precipitation of calcite and Mg^{2+}/K^+ ion exchange results in cluster II
444 Phr composition.

445 All phreatic groundwaters result from a mixing of cluster I and cluster II water that is accom-
446 panied by calcite precipitation, fixation of Mg^{2+} on ion exchange sites against the release of K^+
447 and Na^+ .

448 Moreover, some $CO_{2(g)}$ escapes from the solution at depth, but dissolves much more at the
449 surface. The most complex phenomena occur during the dissolution of Turonian evaporites while
450 CI leaks upwardly towards CT, and from Phr I to Phr II, while the transition from CT to Phr I
451 implies a very limited number of phases. Globally, gypsum dissolution and calcite precipitation
452 processes both act as an inorganic carbon sink.

453 **ACKNOWLEDGEMENTS**

454 The authors wish to thank the staff members of the National Agency for Water Resources
 455 in Ouargla (ANRH) and the Laboratory of Algerian Waters (ADE) for the support provided to
 456 the Technical Cooperation programme within which this work was carried out. Analyses of
 457 ^{18}O were funded by the project CDTN / DDHI (Guendouz and Moulla, 1996). The supports of
 458 University of Ouargla and of INRA for travel grants of R. Slimani and G. Bourrié are gratefully
 459 acknowledged too.

460 **APPENDIX**

461 According to a simple Rayleigh equation, the evolution of the heavy isotope ratio in the
 462 remaining liquid R_l is given by:

$$R_l \approx R_{l,0} \times f_l^{\alpha-1}, \quad (4)$$

463 where f_l is the fraction remaining liquid and α the fractionation factor.

464 The fraction remaining liquid is derived from chloride concentration, as chloride can be con-
 465 sidered as conservative during evaporation: all phreatic waters are undersaturated with respect to
 466 halite, that precipitates only in the last stage. Hence, the following equation holds:

$$f_l \equiv \frac{n_{w,1}}{n_{w,0}} = \frac{[\text{Cl}^-]_0}{[\text{Cl}^-]_1}. \quad (5)$$

467 By taking natural logarithms, one obtains:

$$\ln R_l \approx (1 - \alpha) \times \ln[\text{Cl}^-] + \text{constant}, \quad (6)$$

468 As, by definition,

$$R_l \equiv R_{std.} \times \left(1 + \frac{\delta^{18}\text{O}}{1000}\right), \quad (7)$$

469 one has:

$$\ln R_l \equiv \ln R_{std.} + \ln\left(1 + \frac{\delta^{18}\text{O}}{1000}\right), \quad (8)$$

$$\approx \ln R_{std.} + \frac{\delta^{18}\text{O}}{1000}, \quad (9)$$

470 hence, with base 10 logarithms:

$$\delta^{18}\text{O} \approx 1000(1 - \alpha) \log[\text{Cl}^-] + \text{constant}, \quad (10)$$

$$\approx -\epsilon \log[\text{Cl}^-] + k, \quad (11)$$

471 where as classically defined $\epsilon = 1000(\alpha - 1)$ is the enrichment factor.

472 **References**

- 473 ANRH, 2011. Inventaire des forages de la Wilaya de Ouargla. Rapport technique. Agence Nationale des Ressources
 474 Hydrauliques.
- 475 Aumassip, G., Dagorne, A., Estorges, P., Lefèvre-Witier, P., Mahrouf, F., Nesson, C., Rouvillois-Brigol, M., Trecolle, G.,
 476 1972. Aperçus sur l'évolution du paysage quaternaire et le peuplement de la région de Ouargla. *Libyca*, 205–257.
- 477 Belkhiri, L., Boudoukha, A., Mouni, L., Baouz, T., 2010. Application of multivariate statistical methods and inverse
 478 geochemical modeling for characterization of groundwater — A case study: Ain Azel plain (Algeria). *Geoderma*
 479 159, 390 – 398.
- 480 Belkhiri, L., Mouni, L., Boudoukha, A., 2012. Geochemical evolution of groundwater in an alluvial aquifer: Case of El
 481 Eulma aquifer, East Algeria. *Journal of African Earth Sciences* 66–67, 46 – 55.
- 482 Carucci, V., Petitta, M., Aravena, R., 2012. Interaction between shallow and deep aquifers in the Tivoli Plain (Central
 483 Italy) enhanced by groundwater extraction: A multi-isotope approach and geochemical modeling. *Applied Geochem-*
 484 *istry* 27, 266 – 280. URL: <http://www.sciencedirect.com/science/article/pii/S0883292711004628>,
 485 doi:<http://dx.doi.org/10.1016/j.apgeochem.2011.11.007>.
- 486 Charlton, S., Macklin, C., Parkhurst, D., 1996. PhreeqcI—A graphical user interface for the geochemical computer
 487 program PHREEQC. Rapport technique. U.S. Geological Survey Water-Resources.
- 488 Chellat, S., Bourefis, A., Hamdi-Aïss, a.B., Djerrab, A., 2014. Paléoenvironnemental reconstitution of Mio-pliocenes
 489 sandstones of the lower-Sahara at the base of exoscopic and sequential analysis. *Pensee Journal* 76, 34 – 51.
- 490 Chkir, N., Guendouz, A., Zouari, K., Hadj Ammar, F., Moulla, A., 2009. Uranium isotopes in groundwater from the
 491 continental intercalaire aquifer in Algerian Tunisian Sahara (Northern Africa). *Journal of Environmental Radioac-*
 492 *tivity* 100, 649 – 656. URL: <http://www.sciencedirect.com/science/article/pii/S0265931X09001143>,
 493 doi:<http://dx.doi.org/10.1016/j.jenvrad.2009.05.009>.
- 494 Cornet, A., Gouscov, N., 1952. Les eaux du Crétacé inférieur continental dans le Sahara algérien: nappe dite "Albien",
 495 in: *Congrès géologique international, Alger*. p. 30.
- 496 Dai, Z., Samper, J., Ritzi, R., 2006. Identifying geochemical processes by inverse modeling of multicomponent reactive
 497 transport in the aquia aquifer. *Geosphere* 2, 210–219.
- 498 Deutsch, W., 1997. *Groundwater Chemistry-Fundamentals and Applications to Contamination*. New York.
- 499 Dubief, J., 1953. *Essai sur l'hydrologie superficielle au Sahara*. Direction du service de la colonisation et de
 500 l'hydraulique, Service des études scientifiques.
- 501 Dubief, J., 1963. *Le climat du Sahara*. Hors-série, Institut de recherches sahariennes.
- 502 Eckstein, G., Eckstein, Y., 2003. A hydrogeological approach to transboundary ground water resources and international
 503 law. *American University International Law Review* 19, 201–258.
- 504 Edmunds, W., Guendouz, A., Mamou, A., Moulla, A., Shand, P., Zouari, K., 2003. Groundwater evolution in the
 505 continental intercalaire aquifer of southern Algeria and Tunisia: trace element and isotopic indicators. *Applied*
 506 *Geochemistry* 18, 805–822.
- 507 Fontes, J., Yousfi, M., Allison, G., 1986. Estimation of long-term, diffuse groundwater discharge in the northern sahara
 508 using stable isotope profiles in soil water. *Journal of Hydrology* 86, 315 – 327.
- 509 Foster, S., Margat, J., Droubi, A., 2006. Concept and importance of nonrenewable resources. Number 10 in IHP-VI
 510 *Series on Groundwater, UNESCO*.
- 511 Furon, R., 1960. *Géologie de l'Afrique*. 2eme édition, Payot.
- 512 Güler, C., Thyne, G., 2004. Hydrologic and geologic factors controlling surface and groundwater chemistry in Indian
 513 wells—Owens valley area, southeastern California, USA. *Journal of Hydrology* 285, 177–198.
- 514 Gonfiantini, R., Conrad, G., Fontes, J.C., Sauzay, G., Payne, B., 1975. Étude isotopique de la nappe du Continental
 515 Intercalaire et de ses relations avec les autres nappes du Sahara septentrional. *Isotope Techniques in Groundwater*
 516 *Hydrology* 1, 227–241.
- 517 Guendouz, A., 1985. Contribution à l'étude hydrochimique et isotopique des nappes profondes du Sahara nord-est
 518 septentrional, Algérie. Phd thesis. Université d'Orsay, France.
- 519 Guendouz, A., Michelot, J., 2006. Chlorine-36 dating of deep groundwater from northern Sahara. *Journal of Hydrology*
 520 328, 572–580.
- 521 Guendouz, A., Moulla, A., 1996. Étude hydrochimique et isotopique des eaux souterraines de la cuvette de Ouargla,
 522 Algérie. Rapport technique. CDTN/DDHI.
- 523 Guendouz, A., Moulla, A., Edmunds, W., Zouari, K., Shands, P., Mamou, A., 2003. Hydrogeochemical and isotopic
 524 evolution of water in the complex terminal aquifer in Algerian Sahara. *Hydrogeology Journal* 11, 483–495.
- 525 Hadj-Ammar, F., Chkir, N., Zouari, K., Hamelin, B., Deschamps, P., Aigoun, A., 2014. Hydro-
 526 geochemical processes in the Complex Terminal aquifer of southern Tunisia: An integrated investi-
 527 gation based on geochemical and multivariate statistical methods. *Journal of African Earth Sciences*
 528 100, 81 – 95. URL: <http://www.sciencedirect.com/science/article/pii/S1464343X14001940>,
 529 doi:<http://dx.doi.org/10.1016/j.jafrearsci.2014.06.015>.

- 530 Hamdi-Aïssa, B., Vallès, V., Aventurier, A., Ribolzi, O., 2004. Soils and brines geochemistry and mineralogy of hyper
531 arid desert playa, Ouargla basin, Algerian Sahara. *Arid Land Research and Management* 18, 103–126.
- 532 Kenoyer, G., Bowser, C., 1992. Groundwater chemical evolution in a sandy aquifer in northern Wisconsin. *Water*
533 *Resources Research* 28, 591–600.
- 534 Kuells, C., Adar, E., Udluft, P., 2000. Resolving patterns of ground water flow by inverse hydrochemical modeling in a
535 semiarid Kalahari basin. *Tracers and Modelling in Hydrogeology* 262, 447–451.
- 536 Le Houérou, H., 2009. *Bioclimatology and biogeography of Africa*. Springer Verlag.
- 537 Lelièvre, R., 1969. Assainissement de la cuvette de Ouargla. rapports Géohydraulique n° 2. Ministère des Travaux
538 Publics et de la construction.
- 539 Li, P., Qian, H., Wu, J., Ding, J., 2010. Geochemical modeling of groundwater in southern plain area of Pengyang
540 County, Ningxia, China. *Water Science and Engineering* 3, 282–291.
- 541 Ma, J., Pan, F., Chen, L., Edmunds, W., Ding, Z., Zhou, K., He, J., Zhou, K., Huang, T., 2010. Isotopic and geochemical
542 evidence of recharge sources and water quality in the Quaternary aquifer beneath Jinchang city, NW China. *Applied*
543 *Geochemistry* 25, 996–1007.
- 544 Martinelli, G., Chahoud, A., Dadomo, A., Fava, A., 2014. Isotopic features of emilia-romagna region
545 (north italy) groundwaters: Environmental and climatological implications. *Journal of Hydrology* 519, Part
546 B, 1928 – 1938. URL: <http://www.sciencedirect.com/science/article/pii/S0022169414007690>,
547 doi:<http://dx.doi.org/10.1016/j.jhydrol.2014.09.077>.
- 548 Matiatos, I., Alexopoulos, A., Godelitsas, A., 2014. Multivariate statistical analysis of the hydrogeochemical and isotopic
549 composition of the groundwater resources in northeastern Peloponnesus (Greece). *Science of The Total Environment*
550 476–477, 577 – 590. URL: <http://www.sciencedirect.com/science/article/pii/S0048969714000515>,
551 doi:<http://dx.doi.org/10.1016/j.scitotenv.2014.01.042>.
- 552 Moulias, D., 1927. L'eau dans les oasis sahariennes, organisation hydraulique, régime juridique. Phd thesis. Alger.
- 553 Moulla, A., Guendouz, A., Cherchali, M.H., Chaid, Z., Ouarezki, S., 2012. Updated geochemical and isotopic data
554 from the Continental Intercalaire aquifer in the Great Occidental Erg sub-basin (south-western Algeria). *Quaternary*
555 *International* 257, 64–73.
- 556 OECD, 2008. *OECD Environmental Outlook to 2030. Technical Report 1*. Organisation for Economic Cooperation and
557 Development.
- 558 ONM, 1975/2013. *Bulletins mensuels de relevé des paramètres climatologiques en Algérie*. Office national
559 météorologique.
- 560 OSS, 2003. *Système aquifère du Sahara septentrional*. Technical Report. Observatoire du Sahara et du Sahel.
- 561 OSS, 2008. *Système aquifère du Sahara septentrional (Algérie, Tunisie, Libye): gestion concertée d'un bassin trans-*
562 *frontalier*. Technical Report 1. Observatoire du Sahara et du Sahel.
- 563 Ould Baba Sy, M., Besbes, M., 2006. Holocene recharge and present recharge of the Saharan aquifers — a study by
564 numerical modeling, in: *International symposium - Management of major aquifers*.
- 565 Parkhurst, D., Appelo, C., 2013. Description of Input and Examples for PHREEQC (Version 3) — A computer program
566 for speciation, batch-reaction, one-dimensional transport, and inverse geochemical calculations. Technical Report 6.
567 U.S. Department of the Interior, U.S. Geological Survey. URL: <http://pubs.usgs.gov/tm/06/a43>.
- 568 Plummer, L., Back, M., 1980. The mass balance approach: application to interpreting the chemical evolution of hydro-
569 logical systems. *American Journal of Science* 280, 130–142.
- 570 Plummer, L., Sprinkle, C., 2001. Radiocarbon dating of dissolved inorganic carbon in groundwater from confined parts
571 of the upper Floridan aquifer, Florida, USA. *Journal of Hydrology* 9, 127–150.
- 572 Sharif, M., Davis, R., Steele, K., Kim, B., Kresse, T., Fazio, J., 2008. Inverse geochemical modeling of groundwater
573 evolution with emphasis on arsenic in the Mississippi River Valley alluvial aquifer, Arkansas (USA). *Journal of Hy-*
574 *drology* 350, 41 – 55. URL: <http://www.sciencedirect.com/science/article/pii/S0022169407007093>,
575 doi:<http://dx.doi.org/10.1016/j.jhydrol.2007.11.027>.
- 576 Slimani, R., 2006. Contribution à l'évaluation d'indicateurs de pollution environnementaux dans la région de Ouargla:
577 cas des eaux de rejets agricoles et urbaines. Master's thesis. Université de Ouargla.
- 578 Stumm, W., Morgan, J., 1999. *Aquatic Chemistry: Chemical Equilibria and Rates in Natural Waters*. John Wiley and
579 Sons.
- 580 Thomas, J., Welch, A., Preissler, A., 1989. Geochemical evolution of ground water in smith creek valley - a hydrologi-
581 cally closed basin in central Nevada, USA. *Applied Geochemistry* 4, 493–510.
- 582 Trolard, F., Bourrié, G., Baillieux, A., Buis, S., Chanzy, A., Clastre, P., Closet, J.F., Courault, D., Dangeard, M.L.,
583 Di Virgilio, N., Dussouillez, P., Fleury, J., Gasc, J., Géniaux, G., Jouan, R., Keller, C., Lecharpentier, P., Lecroart, J.,
584 Napoleone, C., Mohammed, G., Oliosio, A., Reynders, S., Rossi, F., Tennant, M., Lopez, J.d.V., 2016. The precos
585 framework: Measuring the impacts of the global changes on soils, water, agriculture on territories to better anticipate
586 the future. *Journal of Environmental Management* 181, 590–601. doi:[10.1016/j.envman.2016.07.002](https://doi.org/10.1016/j.envman.2016.07.002).
- 587 UNESCO, 1972. *Projet ERESS, Étude des ressources en eau du Sahara septentrional*. Technical Report 10. UNESCO.
- 588 Vallès, V., Rezagui, M., Auque, L., Semadi, A., Roger, L., Zougari, H., 1997. Geochemistry of saline soils in two arid

589 zones of the Mediterranean basin. I. Geochemistry of the Chott Melghir-Mehrouane watershed in Algeria. *Arid Soil*
590 *Research and Rehabilitation* 11, 71–84.
591 Zhu, C., Anderson, G., 2002. Environmental application of geochemical modeling. 139, 596–597.

Table 4: Field and analytical data for the Phreatic aquifer (continued).

Locality	Site	Lat.	Long.	Elev.	Date	EC	T	pH	Alk.	Cl ⁻	SO ₄ ²⁻	Na ⁺	K ⁺	Mg ²⁺	Ca ²⁺	Br ⁻
		/m				/mS cm ⁻¹ /°C	/mmol L ⁻¹									
Route Frane	P001	3,572,148	722,366	127	02/02/2013	66.2	28.3	7.2	6.5	468.7	101.5	350.3	26.0	116.2	35.3	
Sebkhet Safioune	P031	3,577,804	720,172	120	1992		23.8	7.3	6.3	481.8	43.4	326.8	12.6	94.2	23.6	
Sebkhet Safioune	P031	3,577,804	720,172	120	02/02/2013	76.0	27.9	8.1	5.9	500.3	110.3	470.5	28.7	79.1	35.5	
Route Frane	P002	3,570,523	722,028	108	1992		23.8	7.8	6.3	522.4	183.0	653.8	10.0	104.7	11.0	
Sebkhet Safioune	P030	3,577,253	721,936	130	1992		23.5	7.7	4.4	527.7	123.5	533.8	11.6	106.2	10.7	
Oum Raneb	P012	3,554,089	718,612	114	25/01/2013	64.1	30.3	7.8	7.8	534.3	20.9	529.6	6.4	19.7	4.7	
Oum Raneb	P012	3,554,089	718,612	114	1992		23.4	7.5	2.7	539.4	60.6	413.6	5.6	112.8	9.4	
ANK Djemel	P423	3,540,881	723,178	102	31/01/2013	90.8	23.5	7.5	6.2	636.5	101.3	495.5	38.3	125.8	30.3	
Said Otba-Chott	P096	3,540,265	724,729	111	1992		23.6	7.7	3.7	645.1	78.5	357.3	6.0	208.4	12.9	
Sebkhet Safioune	P030	3,577,253	721,936	130	03/02/2013	64.7	23.1	7.8	3.7	671.8	90.3	742.9	16.0	41.5	7.7	
N'Goussa	P017	3,560,256	715,781	130	26/01/2013	100.1	31.0	7.1	3.8	679.3	114.1	597.8	10.7	125.9	26.3	
ANK Djemel	P021	3,573,943	723,161	105	1992		23.6	7.4	4.2	700.8	154.5	605.7	53.6	163.1	14.2	
Station de pompage	PL04	3,541,410	723,501	138	1992		23.6	7.4	2.4	716.3	34.8	560.1	7.0	99.6	11.0	
Route Frane	P002	3,570,523	722,028	108	02/02/2013	62.8	26.9	7.6	1.7	748.5	62.6	651.5	14.7	77.7	27.3	
Said Otba-Chott	P096	3,540,265	724,729	111	03/02/2013	68.3	25.9	8.7	1.2	771.0	53.1	615.9	23.5	69.6	50.4	
N'Goussa	P019	3,562,960	717,719	113	1992		23.3	7.7	2.4	779.1	77.1	711.5	9.2	95.6	12.1	
Said Otba(Bab shaa)	P066	3,542,636	718,957	126	03/02/2013	150.6	26.2	7.2	12.3	799.1	283.0	1,249.7	19.0	37.6	18.1	
ANK Djemel	P021	3,573,943	723,161	105	24/01/2013	82.3	29.6	7.6	2.4	800.4	94.4	824.0	11.0	53.4	25.4	
N'Goussa	P018	3,562,122	716,590	110	1992		23.3	7.5	1.2	818.7	81.0	244.2	49.5	319.4	24.8	
Oum Raneb	P162	3,546,133	725,129	98	25/01/2013	160.0	30.7	7.2	2.4	842.8	289.9	1,309.9	13.3	33.5	17.7	
Route Sedrata	P113	3,535,586	714,576	105	1992		23.7	7.7	2.8	954.9	124.9	997.5	13.3	86.7	11.7	
Oum Raneb	PZ12	3,547,234	722,931	110	05/02/2013	114.9	27.4	7.4	2.9	980.1	15.5	930.8	7.5	23.9	14.2	
Hôtel Transat	PL23	3,538,419	720,950	126	1992		23.5	7.4	3.0	1,103.3	94.5	707.8	19.1	270.9	13.3	
Sebkhet Safioune	P023	3,577,198	725,726	99	1992		23.3	7.4	2.3	1,177.0	91.1	1,058.2	11.7	133.5	12.4	
Sebkhet Safioune	P034	3,579,698	725,633	97	05/02/2013	130.0	34.9	8.1	1.8	1,189.1	14.7	1,055.1	18.3	56.4	17.4	
Sebkhet Safioune	P023	3,577,198	725,726	99	05/02/2013	117.9	29.4	8.2	1.9	1,209.3	15.6	1,129.4	8.4	42.9	10.2	
Chott Adjadja	PLX1	3,540,758	726,115	132	1992		23.6	8.0	3.8	1,296.7	134.0	1,458.7	5.2	48.0	4.3	
Sebkhet Safioune	P063	3,545,586	725,667	99	1992		23.5	7.5	1.9	1,379.4	139.6	1,257.4	18.6	182.3	10.0	
LTP06					1992		23.8	7.6	7.8	1,638.7	712.1	2,621.6	41.6	190.5	13.3	
Bamendil	P076	3,540,137	716,721	118	1992		23.5	7.7	5.7	1,743.6	143.4	1,321.9	26.9	331.4	12.3	
El Bour-N'gouca	P007	3,562,236	718,651	129	1992		23.3	7.7	1.4	1,860.5	91.6	1,434.7	26.2	278.8	13.3	
Sebkhet Safioune	P063	3,545,586	725,667	99	05/02/2013	178.9	26.7	7.7	1.4	1,887.9	92.9	1,455.8	26.7	282.9	13.4	
	P044				1992		23.4	7.8	4.5	2,106.1	18.3	1,765.5	27.3	171.2	6.5	
	P093				1992		23.6	7.5	1.5	2,198.6	182.1	1,957.5	29.5	278.2	10.4	
	P042				1992		23.4	7.6	1.1	2,330.9	101.2	1,963.7	52.2	248.1	11.2	
	P068				1992		23.5	7.5	3.4	2,335.7	222.1	2,302.3	26.8	219.9	7.2	
Oum Raneb	PZ12	3,547,234	722,931	110	1992		23.3	7.6	2.2	2,405.6	109.9	2,178.6	25.2	199.4	12.7	
Hassi Debich	P416	3,581,097	730,922	106	1992		23.3	7.8	4.3	2,433.7	178.9	2,361.1	24.3	196.1	9.2	
N'Goussa	P041	3,559,563	716,543	135	1992		23.4	7.9	2.1	2,599.7	324.6	2,879.0	44.6	152.8	11.0	
Sebkhet Safioune	P034	3,579,698	725,633	97	1992		23.3	7.8	1.9	2,752.0	134.1	2,616.8	24.4	180.1	10.5	
	P039				1992		23.4	6.9	1.9	4,189.5	201.4	4,042.6	17.9	257.8	9.2	
Sebkhet Safioune	P074				1992		23.5	6.5	4.2	4,356.5	180.9	2,759.9	57.4	930.1	22.6	
Sebkhet Safioune	P037				1992		23.4	6.9	1.5	4,953.8	184.5	4,611.1	2.9	347.6	7.9	
Sebkhet Safioune	P036				1992		23.4	7.5	1.4	4,972.8	108.1	4,692.2	36.8	221.1	9.6	

For longitude and latitude, the reference is UTM 31 projection for North Sahara 1959 (CLARKE 1880 ellipsoid).

Table 5: Isotopic data ^{18}O and ^3H and chloride concentration in Continental Intercalaire, Complexe Terminal and Phreatic aquifers (sampling campaign in 1992).

Phreatic aquifer											
Piezometer	Cl^- /mmol L $^{-1}$	$\delta^{18}\text{O}$ /‰	^3H /UT	Piezometer	Cl^- /mmol L $^{-1}$	$\delta^{18}\text{O}$ /‰	^3H /UT	Piezometer	Cl^- /mmol L $^{-1}$	$\delta^{18}\text{O}$ /‰	^3H /UT
P007	1.860.5	-2.5	0	PL15	23.5	-7.85	0.6(1)	P074	4.356.4	3.4	6.8(8)
P009	426.9	-6.6	1.2(3)	P066	80.2	-8.1	0.8(1)	PL06	14.2	-8.1	1.0(2)
P506	54.4	-6.8	1.6(3)	PL23	1,103.3	-6.1	0	PL30	24.3	-7.48	2.4(4)
P018	818.7	-2.9	6.2(11)	P063	1,379.3	-3.4	8.7(15)	P002	522.4	-5.7	0.6(1)
P019	779.1	-4.7	5.6(9)	P068	2,335.6	-3.1	8.8(14)	PL21	84.3	-7.7	1.2(2)
PZ12	2,405.5	-2.3	8.1(13)	P030	527.7	-6.6	2.4(4)	PL31	18.9	-7.4	1.6(3)
P023	1,176.9	-2.6	0.2(1)	P076	1,743.5	-5.6	2.8(5)	P433	12.0	-8.8	0
P416	2,433.7	-7.9	5.9(9)	P021	700.7	-5.2	2.6(4)	PL03	84.1	-7.4	1.7(3)
P034	2,752.0	-1.8	5.7(9)	PL04	716.3	-2.9		PL44	109.8	-8.8	1.0(2)
P036	4,972.7	3.3	2.1(4)	P093	2,198.5	-2.6	5.1(8)	PL05	30.9	-7.4	1.9(3)
P037	4,953.8	3.1	1.8(3)	P096	645.1	-6.1	4.8(8)	P408	24.2	-7.9	0
P039	4,189.5	1.0	2.2(4)	PLX1	1,296.6	-5.6	1.1(2)	P116	31.9	-7.2	1.1(2)
P041	2,599.7	-0.6	7.3(13)	PLX2	25.7	-7.6	1.3(2)	LTP 16	213.4	-7.5	1.6(3)
P044	2,106.1	-4.5	2.7(5)	P015	134.7	-6.8	3.0(5)	P117	32.8	-6.9	0.1
P014	336.9	-6.9	2.8(5)	P001	323.6	-4.7	2.5(4)	PL10	35.0	-7.3	0.2(1)
P012	539.3	-6.4	2.2(4)	P100	235.0	-5.8	0	PL25	75.6	-7.4	0.9(2)
P042	2,330.8	2.1	6.0(10)	P056	42.1	-7.0	2.9(5)	LTP30	18.2	-7.5	1.1(2)
P006	19.0	-6.6	0.5(1)	P113	954.9	-4.8	0.8(2)	LTP06	1,638.6	-1.9	2.8(5)
P057	28.2	-7.3	1.1(2)	PLX4	31.5	-7.1	0.3(1)	P031	481.8	-6.1	3.0(5)
P059	20.8	-7.8	0	P115	28.8	-2.5	6.8(12)				

Complexe Terminal aquifer											
Borehole	Cl^- /mmol L $^{-1}$	$\delta^{18}\text{O}$ /‰	^3H /UT	Borehole	Cl^- /mmol L $^{-1}$	$\delta^{18}\text{O}$ /‰	^3H /UT	Borehole	Cl^- /mmol L $^{-1}$	$\delta^{18}\text{O}$ /‰	^3H /UT
D5F80	42.2	-7.9		D1F138	28.9	-8.1	0.7(1)	D2F71	13.5	-8.2	0.6(1)
D3F8	29.8	-8.1	1.4(2)	D3F18	21.7	-8.2	0.2(1)	D7F4	10.6	-8.3	0.1(1)
D3F26	34.7	-8.0	0.8(1)	D3F10	14.3	-7.9	1.5(2)	D2F66	11.0	-8.3	
D4F94	20.1	-8.2	0.6(1)	D6F51	28.4	-7.9	0.7(1)	D1F151	10.8	-8.3	0.4(1)
D6F67	18.8	-8.2	3.7(6)	D1F135	18.1	-8.1	1.1(2)	D6F64	11.4	-8.3	4.3(7)

Continental Intercalaire aquifer											
Borehole	Cl^- /mmol L $^{-1}$	$\delta^{18}\text{O}$ /‰	^3H /UT	Borehole	Cl^- /mmol L $^{-1}$	$\delta^{18}\text{O}$ /‰	^3H /UT	Borehole	Cl^- /mmol L $^{-1}$	$\delta^{18}\text{O}$ /‰	^3H /UT
Hadeb I	5.8	-8.0	0	Hadeb II	6.2	-7.9	0.1(1)	Aouinet Moussa	6.5	-7.9	1.1(2)

Table 6: Statistical parameters for Continental Intercalaire (CI), Complexe Terminal (CT) and Phreatic (Phr) aquifers samples selected on the basis of $\delta^{18}\text{O}$ and Cl^- data (see text).

Aquifer	Size	Parameter	EC /mS cm $^{-1}$	T /°C	pH	Alk.	Cl^-	SO_4^{2-}	Na^+	K^+	Mg^{2+}	Ca^{2+}
			/mmol/L									
CI	11	Average	2.2	49.0	7.5	2.3	11.0	4.7	10.3	0.5	3.6	2.4
CI	11	Stdd. dev.	0.3	2.0	0.2	1.0	4.6	2.5	4.6	0.2	2.0	1.8
CT	50	Average	3.2	23.0	7.8	2.3	20.0	8.9	17.0	1.0	5.5	5.6
CT	50	Stdd. dev.	1.1	2.4	0.4	0.8	7.0	2.6	6.0	0.8	2.2	1.7
Phr cluster I	30	Average	3.9	24.0	7.9	2.3	24.7	11.8	24.2	2.1	7.2	5.3
Phr cluster I	30	Stdd. dev.	1.3	1.3	0.4	1.0	6.9	3.4	11.0	1.7	5.0	2.7
Phr cluster II	3	Average		23.4	7.0	2.4	4,761.0	158.0	4,021.0	32.4	500.0	13.0
Phr cluster II	3	Stdd. dev.		0.1	0.5	1.6	350.0	43.0	1,093.0	28.0	378.0	8.0

Table 7: Summary of mass transfer for geochemical inverse modeling. Phases and thermodynamic database are from Phreeqc 3.0 (Parkhurst and Appelo, 2013).

Phases	Stoichiometry	CI/CT	CT/Phr I	Rainwater/P036	PhrI/PhrII 60%/40%
Calcite	CaCO ₃	—	-6.62×10^{-6}	-1.88×10^{-1}	-2.26×10^{-1}
CO ₂ (g)	CO ₂	-6.88×10^{-5}	—	8.42×10^{-4}	5.77×10^{-4}
Gypsum	CaSO ₄ · 2 H ₂ O	4.33×10^{-3}	—	1.55×10^{-1}	1.67×10^{-1}
Halite	NaCl	7.05×10^{-3}	3.76×10^{-3}	6.72	1.28
Sylvite	KCl	2.18×10^{-3}	1.08×10^{-3}	4.02×10^{-1}	—
Bloedite	Na ₂ Mg(SO ₄) ₂ · 4 H ₂ O	—	1.44×10^{-3}	—	—
Huntite	CaMg ₃ (CO ₃) ₄	—	—	4.74×10^{-2}	5.65×10^{-2}
Ca ion exchange	CaX ₂	-1.11×10^{-3}	—	—	—
Mg ion exchange	MgX ₂	1.96×10^{-3}	—	1.75×10^{-1}	-2.02×10^{-1}
Na ion exchange	NaX	—	—	—	3.92×10^{-1}
K ion exchange	KX	-1.69×10^{-3}	—	-3.49×10^{-1}	1.20×10^{-2}

Values are in mol/kg (H₂O). Positive (mass entering solution) and negative (mass leaving solution) phase mole transfers indicate dissolution and precipitation, respectively; — indicates no mass transfer.

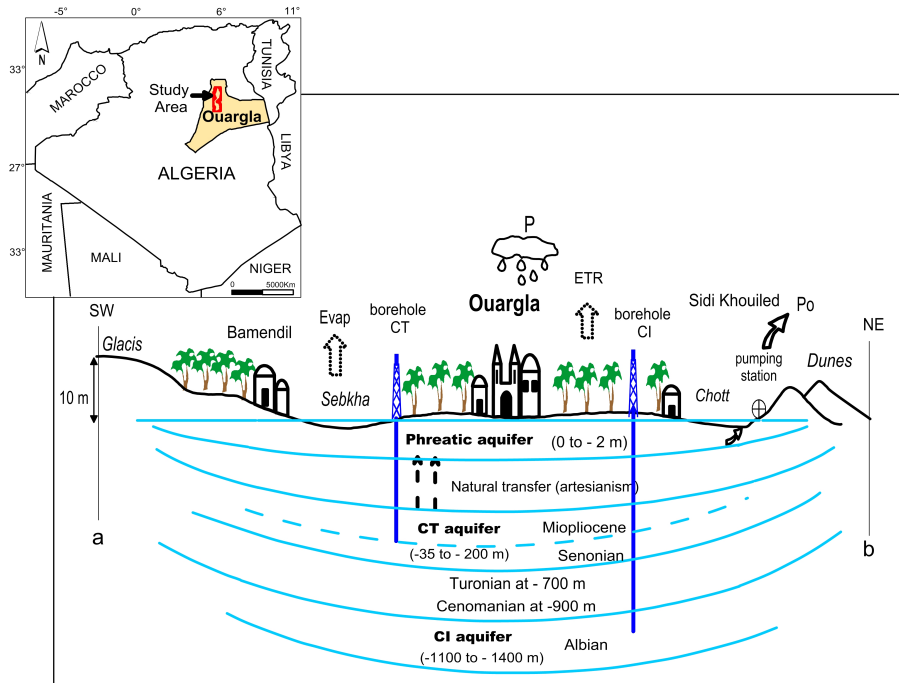


Figure 1: Location and schematic relations of aquifers in Ouargla. Blue lines represent limits between aquifers, and the names of aquifers are given in bold letters; as the limit between Senonian and Mio-pliocene aquifers is not well defined, a dashed blue line is used. Names of villages and cities are given in roman (Bamendil, Ouargla, Sidi Khouiled), while geological/geomorphological features are in italic (Glacis, Sebkhia, Chott, Dunes). Depths are relative to the ground surface. Letters a and b refer to the cross section (fig. 2) and to the localisation map (fig. 3).

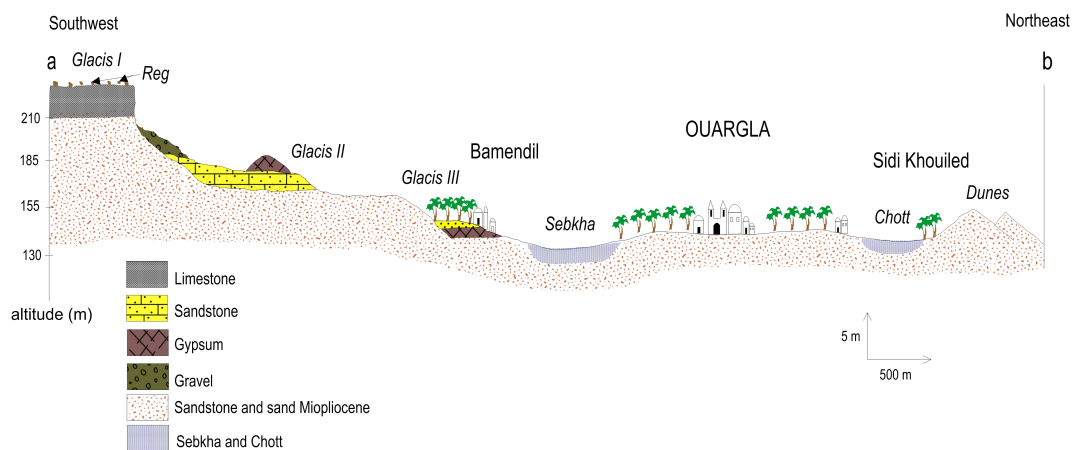


Figure 2: Geologic cross section in the region of Ouargla. The blue pattern used for Chott and Sebkhia correspond to the limit of the saturated zone.

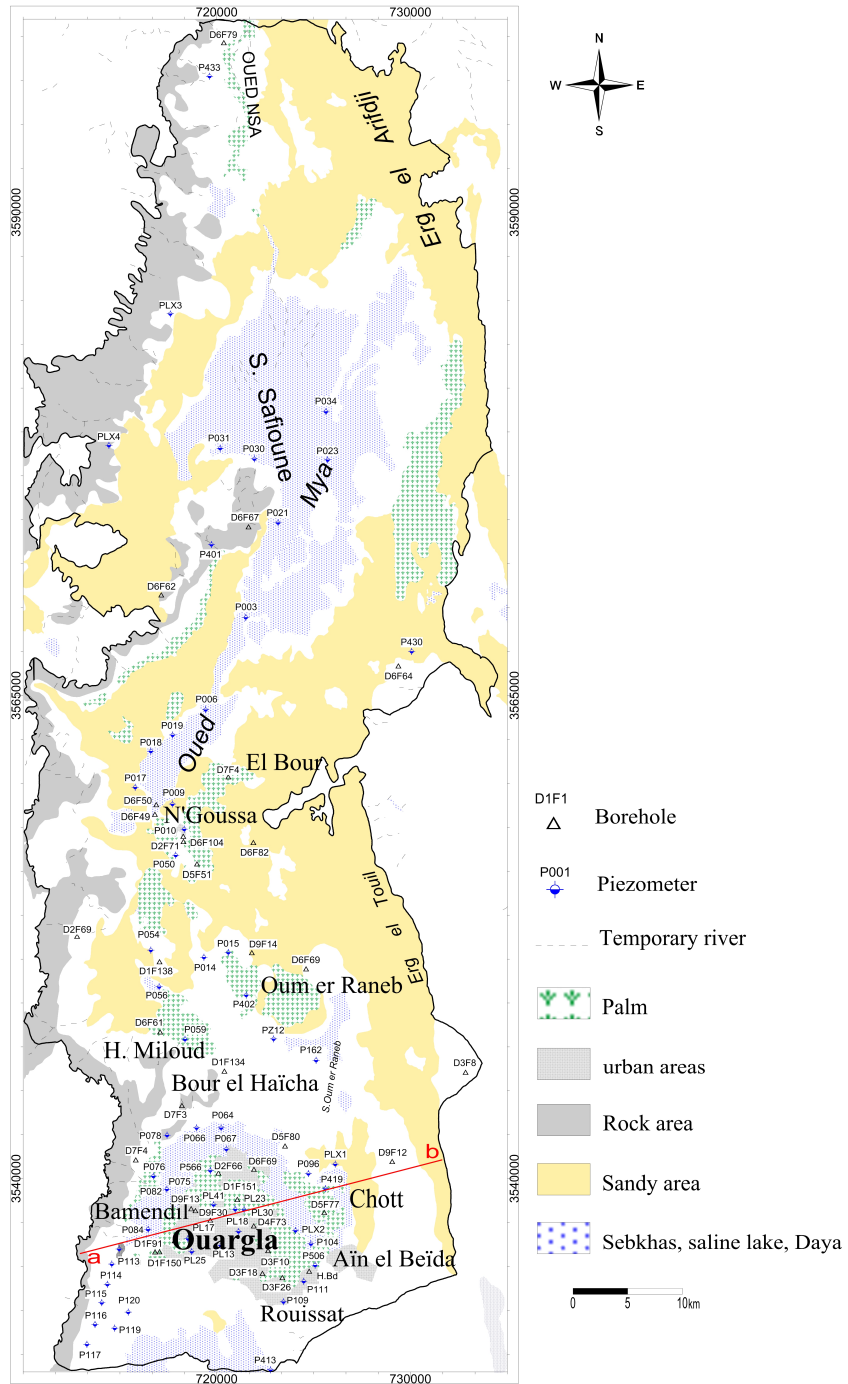


Figure 3: Location map of sampling points

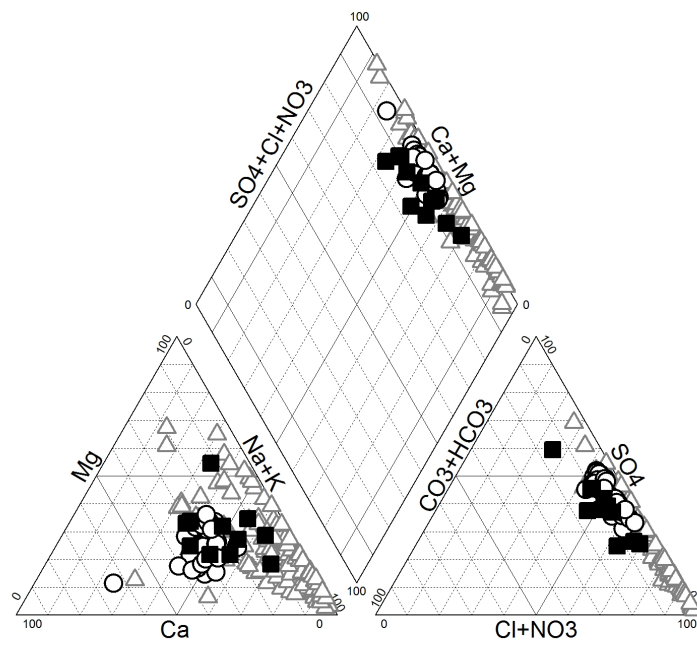
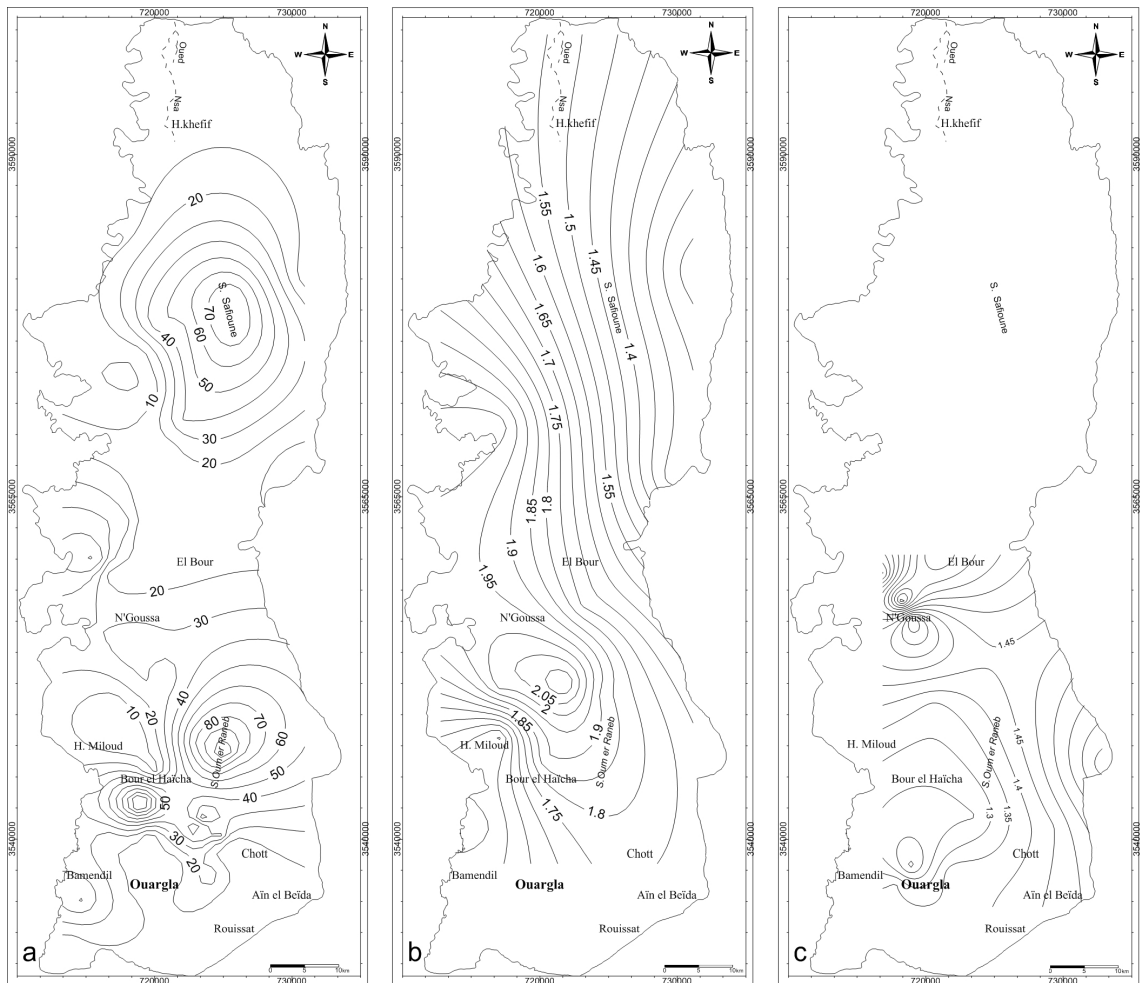


Figure 4: Piper diagram for Continental Intercalaire (filled squares), Complexe Terminal (open circles) and Phreatic aquifer (open triangles).



5

Figure 5: Contour maps of the salinity (expressed as global mineralization) in the aquifer system, (a) Phreatic aquifer; (b) and (c) Complex Terminal [(b) Mio-pliocene and (c) Senonian]; figures are isovalues of global mineralization (values in g/L).

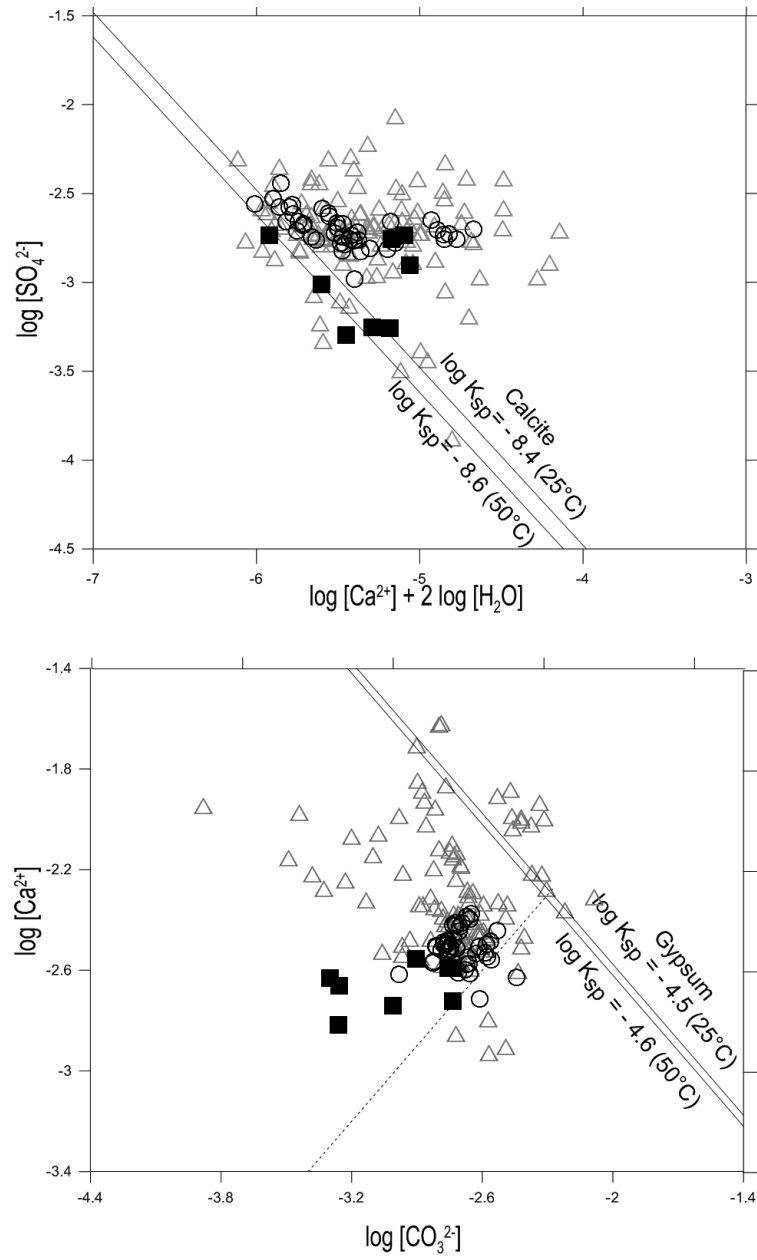


Figure 6: Equilibrium diagrams of calcite (top) and gypsum (bottom) for Continental Intercalaire (filled squares), Complexe Terminal (open circles) and Phreatic aquifer (open triangles). Equilibrium lines are defined as: $\log[\text{Ca}^{2+}] + \log[\text{CO}_3^{2-}] = \log K_{sp}$ for calcite, and $\log[\text{Ca}^{2+}] + 2 \log[\text{H}_2\text{O}] + \log[\text{SO}_4^{2-}] = \log K_{sp}$ for gypsum.

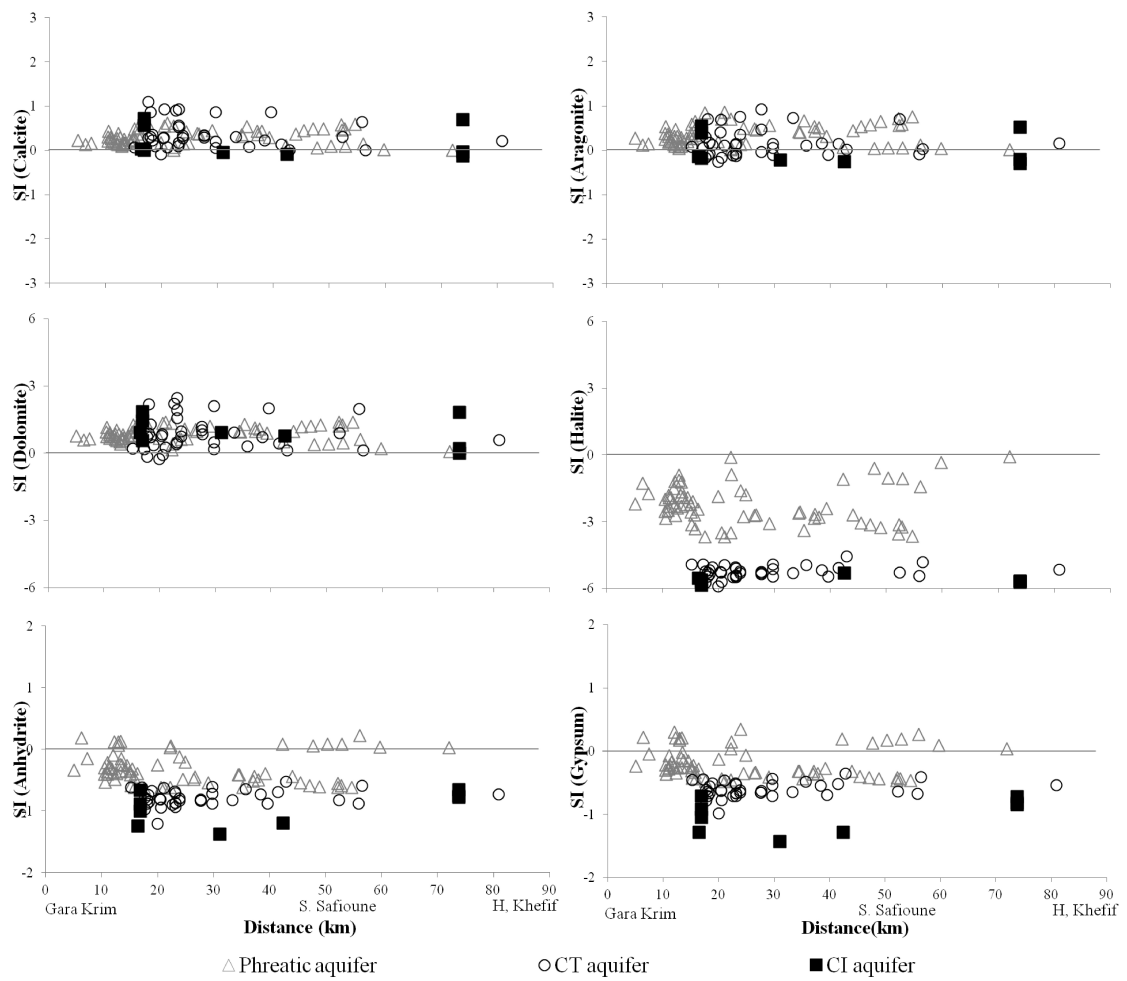


Figure 7: Variation of saturation indices with distance from south to north in the region of Ouargla.

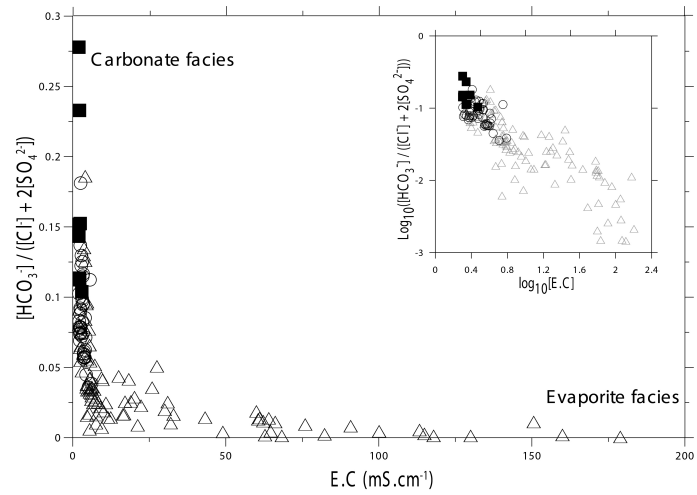


Figure 8: Change from carbonate facies to evaporite from Continental Intercalaire (filled squares), Complexe Terminal (open circles) and Phreatic aquifer (open triangles).

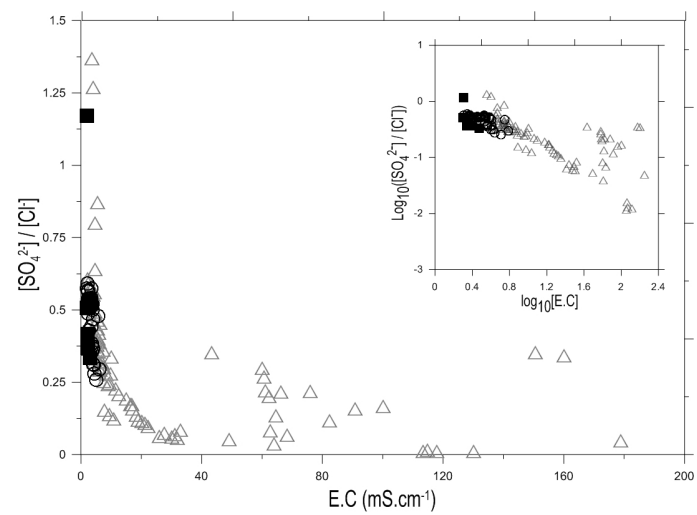


Figure 9: Change from sulfate facies to chloride from Continental Intercalaire (filled squares), Complexe Terminal (open circles) and Phreatic aquifer (open triangles).

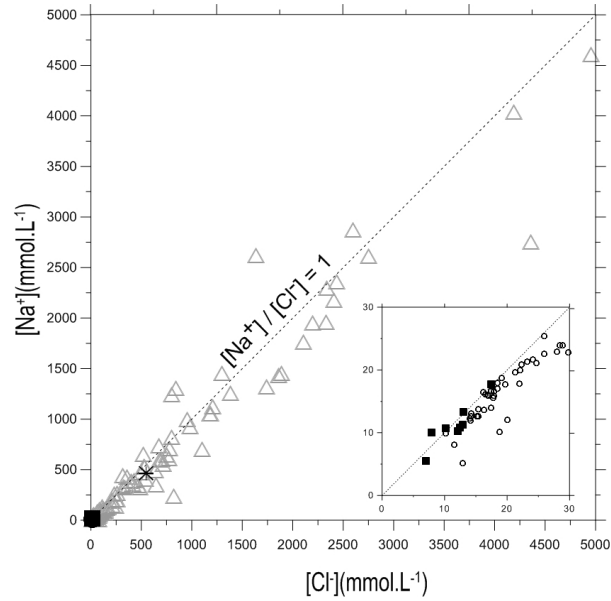


Figure 10: Correlation between Na^+ and Cl^- concentrations in Continental Intercalaire (filled squares), Complex Terminal (open circles) and Phreatic aquifer (open triangles). Seawater composition (star) is $[Na^+] = 459.3$ mmol.L⁻¹ and $[Cl^-] = 535.3$ mmol.L⁻¹ (Stumm and Morgan, 1999, p.899).

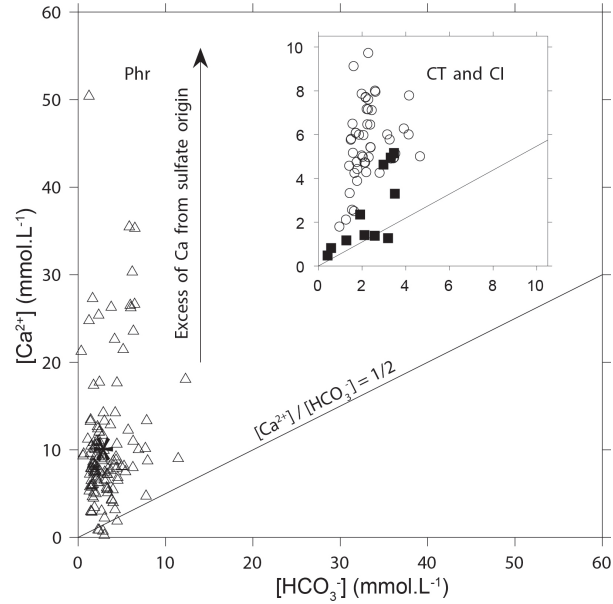


Figure 11: Calcium vs. HCO_3^- diagram in Continental Intercalaire (filled squares), Complex Terminal (open circles), Phreatic aquifer (open triangles) and Seawater composition (star) is $[Ca^{2+}] = 10.2$ mmol.L⁻¹ and $[HCO_3^-] = 2.38$ mmol.L⁻¹ (Stumm and Morgan, 1999, p.899).

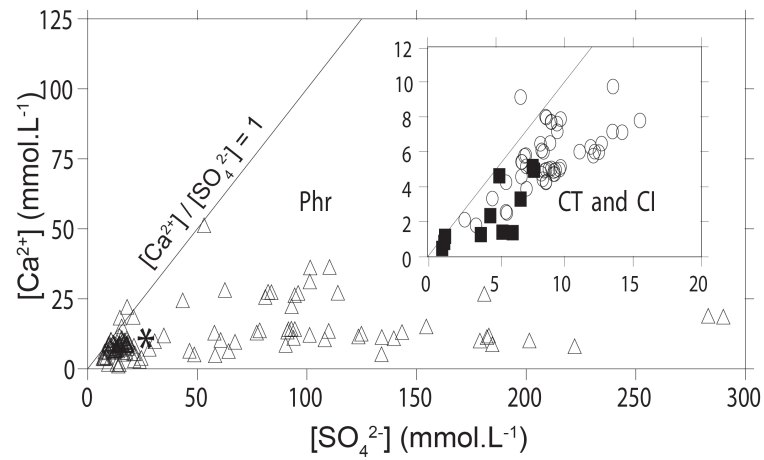


Figure 12: Calcium vs. SO_4^{2-} diagram in Continental Intercalaire (filled squares), Complexe Terminal (open circles), Phreatic aquifer (open triangles) and Seawater composition (star) is $[\text{Ca}^{2+}] = 10.2 \text{ mmol L}^{-1}$ and $[\text{SO}_4^{2-}] = 28.2 \text{ mmol L}^{-1}$ (Stumm and Morgan, 1999, p.899).

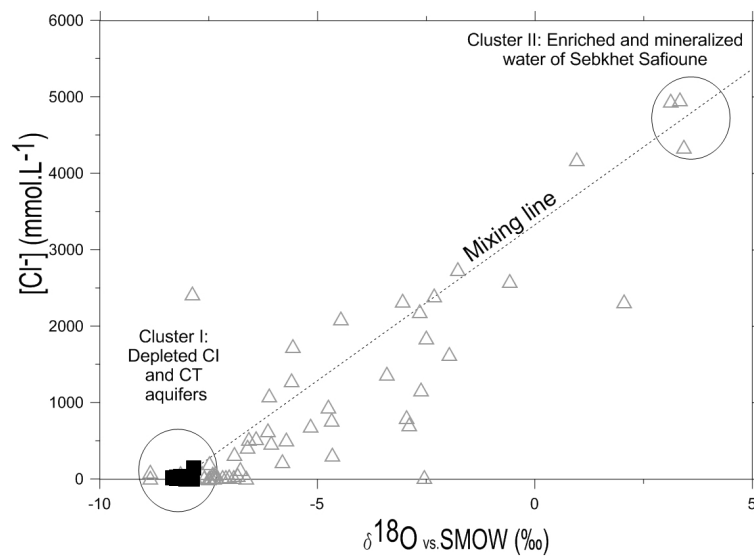


Figure 13: Chloride concentration versus $\delta^{18}\text{O}$ in Continental Intercalaire (filled squares), Complexe Terminal (open circles) and Phreatic aquifer (open triangles) from Ouargla.

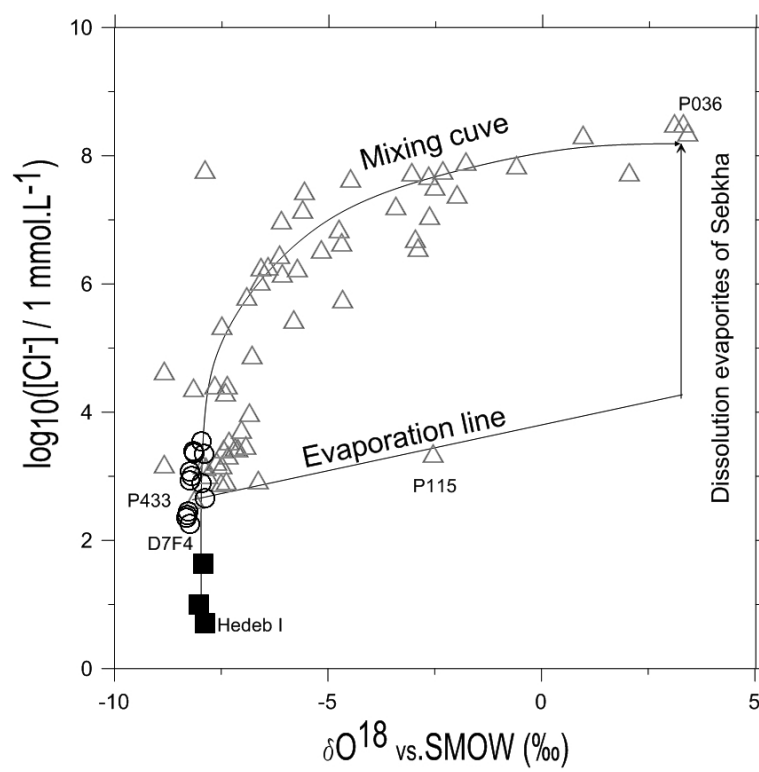


Figure 14: Log $[\text{Cl}^-]$ concentration versus $\delta^{18}\text{O}$ in Continental Intercalaire (filled squares), Complexe Terminal (open circles) and Phreatic aquifer (open triangles) from Ouargla.